Deterministic Chaos and Noise in Three *In Vitro* Hippocampal Models of Epilepsy

Marc W. Slutzky,[1] Predrag Cvitanović,[2] and David J. Mogul[1]

[1]Departments of Biomedical Engineering and [2]Physics and Astronomy, Northwestern University, Evanston, IL

Abstract—Recent reports have suggested that chaos control techniques may be useful for electrically manipulating epileptiform bursting behavior in neuronal ensembles. Because the dynamics of spontaneous *in vitro* bursting had not been well determined previously, analysis of this behavior in the rat hippocampus was performed. Epileptiform bursting was induced in transverse rat hippocampal slices using three experimental methods. Slices were bathed in artificial cerebrospinal fluid containing: (1) elevated potassium ($[K^+]_o = 10.5$ mM), (2) zero magnesium, or (3) the $GABA_A$-receptor antagonists bicuculline (20 μM) and picrotoxin (250 μM). The existence of chaos and determinism was assessed using two different analytical techniques: unstable periodic orbit (UPO) analysis and a new technique for estimating Lyapunov exponents. Significance of these results was assessed by comparing the calculations for each experiment with corresponding randomized surrogate data. UPOs of multiple periods were highly prevalent in experiments from all three epilepsy models: 73% of all experiments contained at least one statistically significant period-1 or period-2 orbit. However, the expansion rate analysis did not provide any evidence of determinism in the data. This suggests that the system may be globally stochastic but contains local pockets of determinism. Thus, manipulation of bursting behavior using chaos control algorithms may yet hold promise for reverting or preventing epileptic seizures. © *2001 Biomedical Engineering Society.* [DOI: 10.1114/1.1380419]

Keywords—Chaos, Hippocampus, Epilepsy, Nonlinear, Unstable periodic orbit, Lyapunov exponent, Determinism, Potassium, GABA, Magnesium, Chaos, Electrophysiology, Brain.

INTRODUCTION

Epilepsy afflicts between 1% and 2% of the world's population. While many antiepileptic drugs currently exist, at least 20% of all epileptic patients are still not kept seizure-free by pharmacological treatment. For many of these patients, the only remaining option is surgical resection of the seizure focus. Schiff *et al.*[24] have demonstrated that it may be possible to apply techniques from nonlinear dynamics to manipulate *in vitro* epileptiform bursting. These bursts are thought to be analogous to interictal spikes—those seen on an EEG between seizure episodes—and are thus a hallmark of epilepsy.[16] It has been postulated that this bursting is chaotic and hence could be controlled using chaos control techniques.[24] Although simple periodic pacing has been shown to be capable of preventing ictal seizure activity *in vitro*,[11] using such a protocol *in vivo* might kindle new epileptic foci resulting in more seizures rather than fewer. The advantage of using chaos control is that the stimuli would be applied relatively infrequently thereby reducing the likelihood of inducing new seizures.

There are, in general, three essential ingredients to a chaotic system: determinism, aperiodicity, and sensitive dependence on initial conditions.[29] In contrast to a stochastic system, a deterministic system follows some mathematical relationship and in this sense is predictable. In a chaotic system, however, this predictability is limited by sensitive dependence on initial conditions. The evolution of a system's behavior over time is represented by a trajectory, or orbit, in state space. In a chaotic system, two trajectories that start close to each other will diverge exponentially over time. This divergence can be quantified by calculating the Lyapunov exponents of the system. A chaotic trajectory can also be described as wandering along a path of an infinite amount of unstable periodic orbits (UPOs).[8] Detection of UPOs in a system is an indication that the system contains determinism and may be chaotic.

Significant efforts have been made to try to characterize neuronal behavior using nonlinear dynamical systems theory.[2,17] UPOs have been detected in multiple neuronal systems, the first being the crayfish photoreceptor.[17] Much of the research on dynamics in epilepsy has focused on calculating the correlation dimension[6,35] which can be misleading in practice because of the need for many assumptions and the prevalence of false positive results.[19] Some have searched for chaos by calculating Lyapunov exponents of electroencephalogram (EEG) data,[21,31] but the algorithms used have several drawbacks,[31] notably poor performance in noisy systems (i.e., ones that have a substantial stochastic component in

addition to determinism). Studies with these techniques have provided evidence both supporting[18,21] and contradicting[31] the existence of nonlinear determinism in EEG seizure activity. One group has found evidence of a few period-1 orbits in epileptic EEG recordings from three human subjects.[13] Another has found several period-1 orbits in both the high-$[K^+]_o$ *in vitro* model and in human epileptic EEG recordings as well as a few orbits of periods 2 and 3 in intracellular recordings from CA1 neurons in normal ACSF.[27]

Little prior evidence exists as to whether spontaneous *in vitro* bursting contains determinism or is purely stochastic in nature.[27] To the best of our knowledge, only two reports have investigated nonlinear characteristics of the high-$[K^+]_o$ *in vitro* model of epilepsy. In one,[23] three types of nonlinear prediction were used to analyze data from six hippocampal slices; only one slice showed evidence of determinism. The other report[27] found evidence of unstable period-1 orbits in about half of the experiments in extracellular potassium concentrations of 7.5–9.5 mM and in 91% of the experiments at 10.5 mM $[K^+]_o$. This was the first evidence for determinism in epileptiform bursting in the high-$[K^+]_o$ model; however, these findings alone were not sufficient to prove chaos and were more restricted by the cellular mechanisms underlying the bursting activity since only one burst-induction protocol was used.

We used three different experimental protocols to elicit epileptiform bursting, in order to investigate whether different mechanisms underlying spontaneous bursting created significant differences in system dynamics: (1) high-$[K^+]_o$;[20] (2) zero-$[Mg^{2+}]_o$;[33] and (3) the γ-amino-butyric acid (GABA$_A$, an inhibitory neurotransmitter) receptor antagonists picrotoxin and bicuculline.[5] We analyzed this bursting using two different measures of chaos: UPO detection and a novel technique, designed for data from noisy systems, that assesses deterministic expansion.

METHODS

Experimental Protocols

Hippocampal slices were obtained from 20- to 25-day-old male Sprague–Dawley rats (Harlan). Animals were anesthetized with isoflurane by inhalation and then decapitated. The brain was rapidly excised, hemisected at the central fissure, and placed in cold (4 °C) artificial cerebrospinal fluid (ACSF) containing (in mM): NaCl 130, NaHCO$_3$ 24, D-Glucose 10, MgSO$_4$ 1.3, NaH$_2$PO$_4$ 1.25, KCl 3.5, CaCl$_2$ 2.4 and gassed with 95% O$_2$/5% CO$_2$. Both hippocampi were dissected free and 400 μm transverse slices were cut using a vertical tissue chopper (Stoelting). Slices were stored in the bubbled ACSF at room temperature (~22 °C) for at least 1 h and then transferred as needed to a submersion chamber.

Field potential (extracellular) measurements were recorded in stratum pyramidale of the CA3 region. Recordings were made using glass microelectrodes (2–4 MΩ) pulled from borosilicate glass capillaries and filled with 2 M NaCl. Signals from the electrodes were bandpass filtered (0.3 Hz $< f <$ 3 kHz) using an ac differential amplifier (DAM 80, World Precision Instruments). The signals were then digitized (at 10 kHz) with a Digidata 1200 A/D converter board and acquired using AXOBASIC software (Axon Instruments). The viability of the slice was assessed by stimulating the Schaffer collaterals and recording excitatory postsynaptic potentials (EPSPs) from stratum radiatum of CA1. Only slices with EPSP amplitudes greater than 0.4 mV were used.

Epilepsy Models

Slices were placed in the recording chamber ($T = 34 \pm 1$ °C) for at least 30 min prior to initiation of the experimental protocol. Slices were then exposed to the experimental solution for 30 min prior to initiation of recording. Bursts were generated using three different *in vitro* models of epilepsy: (1) ACSF containing elevated $[K^+]_o$ (10.5 mM); (2) Mg^{2+}-free ACSF; or (3) 20 μM bicuculline methochloride (Sigma) and 250 μM picrotoxin (Sigma) added to ACSF containing 1.2 mM $[Ca^{2+}]$ and 5 mM $[K^+]$. The changes in calcium and potassium concentrations in the third model were necessary in order to attain a burst rate sufficiently fast to achieve an acceptable level of accuracy in the data analysis. Data were recorded and analyzed off-line. Bursts were detected using a combination voltage- and time-threshold software algorithm. Criteria used to identify a burst were as follows: (1) the waveform must exceed the voltage threshold (0.03–0.05 mV) for more than 16 ms but less than 1000 ms, (2) bursts must be at least 250 ms apart, and (3) the wave form cannot dip below the threshold for more than 20 ms at a time (this allowed for multiple spikes riding on top of a burst). The time between bursts, called interburst interval (IBI, see Fig. 1), was the system parameter used to characterize behavior.

Mathematical Methods

The dynamics of the bursting activity was characterized using a measure similar to Lyapunov exponents[1] and unstable periodic orbits.[27] These two measures provide both global and local information about a system's behavior in state space. A chaotic system possesses the seemingly paradoxical property of being locally unstable but yet globally recurrent, i.e., the system returns repeatedly to certain states. The existence of a positive Lyapunov exponent in a system defines that system's
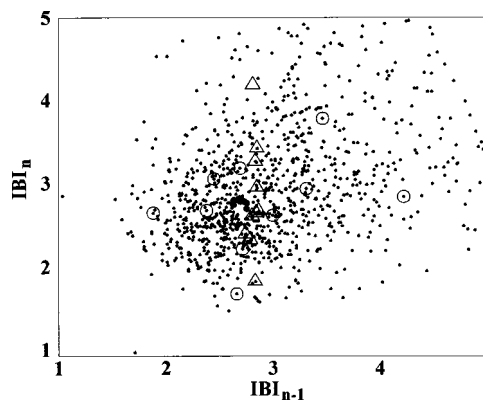
A

0.5 mV

100 ms

B

5 s

C

D
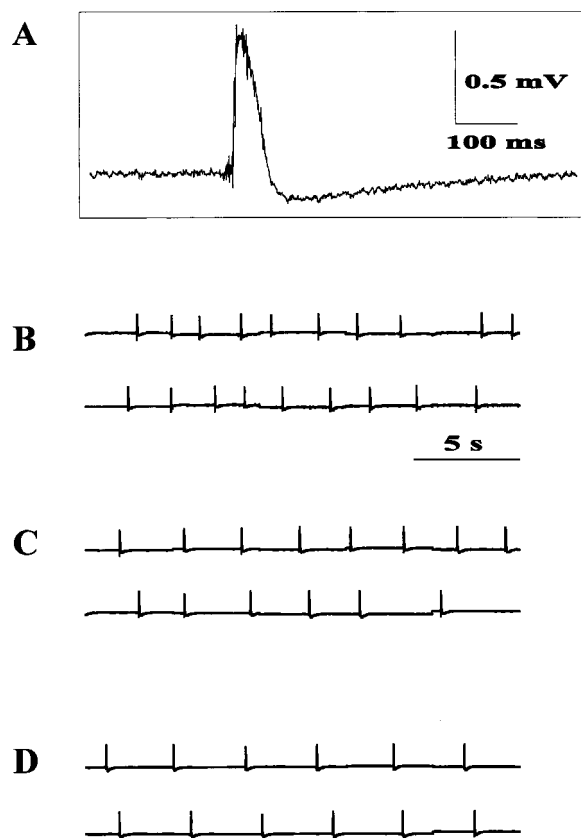
FIGURE 1. Spontaneous bursting elicited by three different experimental techniques recorded extracellularly in CA3 pyramidal layer of the rat transverse hippocampal slice. (A) The typical extracellular recording of a spontaneous burst, generated by the high-$[K^+]_o$ model. (B)–(D) Time series data of spontaneous bursts generated by (B) high-$[K^+]_o$ (10.5 mM), (C) zero-$[Mg^{2+}]_o$, and (D) $GABA_A$ receptor blockade using bicuculline (20 μM) and picrotoxin (250 μM). Each pair of traces is contiguous in time.

FIGURE 2. Rapid expansion of a small cluster of points for data from a high-$[K^+]_o$ experiment. The whole attractor (·) is shown in delay coordinates. The initial cloud of points (●) expands rapidly after one iteration (△) and covers almost the whole attractor width after two iterations (○).

behavior as chaotic.[29] Furthermore, the existence of unstable periodic orbits in a system implies that the system is deterministic and likely chaotic.[3]

Analysis Concepts

State Space and Embedding. Periodic orbits can be stable or unstable. Stable periodic orbits attract other nearby trajectories, while UPOs repel trajectories in at least one direction and may attract or repel them in other directions. Chaotic trajectories can be characterized by a "skeleton" of UPOs that they approach and recede from as time evolves.[3] Using time-delay embedding, scalar data can be converted into vectors which form a more complete representation of the system in state space. This embedding has been shown to preserve the geometric and dynamical properties of the system.[30] For all of the data analyses in this study, IBIs were first embedded into two-dimensional vectors consisting of the current and

next IBIs (e.g., see Fig. 2). Such IBI embeddings have also been shown to be sufficient to characterize most of the original system's dynamical behavior.[9,22]

Surrogate Data. Most natural systems have some amount of noise in them, and it has been hypothesized that neurons fire in a purely stochastic manner. To provide evidence that the data indeed contained a deterministic component and not merely stochastic noise, the method of surrogate data was used.[32] Surrogate data sets were created by randomizing the order of a data set. The same measures were then computed for the surrogates and the results compared with the data. This permitted testing the null hypothesis that any apparent structure in the data can be accounted for by a purely stochastic process.

Lyapunov Exponent Estimates. Exponential divergence of two nearly identical points in state space can be quantified by the Lyapunov exponents of a system. A positive exponent signifies exponential expansion and thus chaos. An *m*-dimensional system will in general have *m* Lyapunov exponents associated with it. However, for our purposes it was sufficient to calculate the largest Lyapunov exponent, for if the largest exponent is positive, the system is chaotic.

For small and noisy data sets, the computation of Lyapunov exponents can be very difficult. Most algorithms for measuring the largest Lyapunov exponent look at a small group of points that are close neighbors in state space and examine how they spread out as time evolves. If there are not a sufficiently large number of points in the data, however, one must increase the initial neighborhood size in order to include a sufficient number of points in the calculation. This can create erroneous expansion rates since points that are not truly neighbors

in state space are being treated as such. Also, noise may cause points that appear close together to diverge rapidly as well.

To overcome these obstacles, a new method of detecting determinism based on short-time expansion rates was developed and used. While the resulting measure of expansion is not a Lyapunov exponent, it would converge to the largest Lyapunov exponent in a noiseless system. Therefore, for the sake of convenience, our "expansion rate" will be referred to as a Lyapunov exponent estimate. This method is described more fully in the "Technical Details" section below.

Unstable Periodic Orbits. Lyapunov exponents are extracted from full data sets and are thus global measures of chaotic dynamics. To characterize the system's dynamics on a local scale, we also searched the data for the presence of unstable periodic orbits. The existence of a few UPOs in experimental data is not sufficient to prove that a system is chaotic; however, it does imply determinism and strongly suggests the presence of chaos in the system. Moreover, it has been shown[3] that good estimates of the dynamics of a system can be made using only the low-period UPOs, which are the easiest to detect. Furthermore, the presence of low-period UPOs is a prerequisite for the successful application of most forms of chaos control.[26]

The recently introduced method of So *et al.*[28] was used to search for low-period orbits. This technique uses a transformation to concentrate data around UPOs thus creating peaks in the histogram of the transformed data that correspond to the locations of the UPOs. This allows the simple detection of UPOs by locating the peaks in the distribution of the transformed data. The significance of these peaks was assessed using surrogate data.

Technical Details of the Analysis

Surrogate Data. Two types of surrogate data were used. For the Lyapunov exponent computations, surrogate data sets were created by shuffling the order of the IBIs using a Gaussian distribution.[23] These surrogates maintained the amplitude distribution of the original data while removing any correlation.

For the UPO analysis, amplitude-adjusted Fourier transform (AAFT) surrogates were used.[32] First, a Gaussian-distributed random set x was created and rank ordered according to the original data, and its Fourier transform was computed. Then the phases of this set were randomized, and the inverse Fourier transform was performed, giving set x_r. Finally, the original data set was rank-ordered according to x_r, producing the surrogate. These surrogates thus maintained the amplitudes and approximate power spectrum of the original data.

Other types of surrogates have been suggested as being more appropriate for use in detecting UPOs.[10] These include the Gaussian-shuffled (or simple-shuffled, SS) surrogates, which were used in the Lyapunov exponent calculations. To further confirm the significance of the UPOs, the SS surrogates were also used for analyzing several data sets. The issue of the appropriate surrogate type for validating UPOs in ISI series is controversial, as each type of surrogate has its own advantages and flaws.[25] However, the use of two different types of surrogates should help reduce the chance of error due to the type of surrogate.

Lyapunov Exponents. Many algorithms exist for calculating the Lyapunov exponents from time series data.[1,34] We first used the method derived by Kantz,[12] which is similar to the method of Wolf *et al.*[34] but is more robust to noise. The algorithm measures the rate at which two points in state space separate over varying amounts of time (τ). Averaging over all points in the state space, and the use of all nearest neighbors helps make this algorithm particularly robust to some noise. Averaging over the entire data set means that the Lyapunov exponent λ is a global measure of chaos.

The Lyapunov calculations were tested for significance using SS surrogates. Five surrogates were created for each experiment, and $\lambda \pm s$ (the standard error) was calculated for each surrogate. A weighted ratio was then calculated for each group of surrogates. This ratio was compared to the ratio λ/s for each data set, thus providing a measure of statistical significance for the null hypothesis that the experimental data were no different from Gaussian noise.

The algorithm was successfully tested on the Hénon map, a chaotic system conventionally used to benchmark such algorithms. The algorithm calculated an exponent of 0.415 for 2000 points of the Hénon map with 1% Gaussian noise added, which was in close agreement with the accepted value of 0.4169.[12] In all of the calculations with this method, initial neighborhood size was 0.1 s and τ varied from 2 to 21. However, when the IBI data were examined more closely, it was noted that points in the initial neighborhood expanded very quickly, in fact, they typically spread out to separations exceeding half the size of the entire attractor within one or two iterates. (In this article, we use the term attractor in a loose sense to refer to the region that no point in the data set exits.) Once the points had spread this far apart, there was not much room left for them to spread, so using $\tau > 2$ would be misleading. In other words, there was no conceivable way in which the expansion rate of IBI data could be measured over a long time span, which is required to properly evaluate Lyapunov exponents. Therefore, a different approach to estimating expansion rates was developed.

Short-Time Expansion Measure. In one-dimensional systems the Lyapunov exponent can be computed by integrating over the instantaneous expansion rate weighted by the local trajectory visitation rate (i.e., probability density function). The new method mimics this for higher-dimensional systems, and surmounts the obstacle of extremely rapid expansion by examining the ratio of distances between nearby points after only one iterate. The method estimated the maximal Lyapunov exponent by using a spatial average of the many local expansion rates on an attractor. A fixed number of nearest neighbors was found for every point in the data set. The resulting cloud of points were then fit to an ellipse using principal components analysis (PCA). The largest principal component was the variance along the major axis of the best-fit ellipse and thus its square root (standard deviation) served as a measure of the initial ''spread'' between the points. The points in the neighborhood were then evolved one time step into the future. These points were again fit to an ellipse using PCA, and the variance along the major axis was obtained. The ratio of the final to the initial principal components then provided an estimate of the one-step expanding eigenvalue. The natural logarithm of the square root of this ratio was the estimated local Lyapunov exponent. The global Lyapunov exponent was then obtained by averaging the local estimates. That is,

$$L_{ave} = \frac{1}{N} \sum_{i=1}^{N} \lambda_i, \quad \lambda_i = \ln\left(\sqrt{\frac{p_1}{p_0}}\right), \qquad (1)$$

where p_0 and p_1 were the largest principal components of the initial and iterated clouds of points, respectively; N was the total number of points; λ_i was the local expansion rate; and L_{ave} was the estimated Lyapunov exponent for the whole set. The expectation was that for deterministic systems, small neighborhoods of points would not spread out as quickly as in stochastic systems after only one time step. If the system contained a strong stochastic component, the points would likely spread out over most if not all of the attractor after only one time step. For a cloud of neighboring points, the noise should partially average out in this calculation, leaving primarily the deterministic component. Therefore, the expectation was that the local expansion rate, L_{ave}, should be smaller for a deterministic system than for a stochastic system. In this approach the determinism was discriminated from noise by comparing L_{ave} for a data set against L_{ave} for corresponding surrogate data.

The estimate of the Lyapunov exponent produced by this method was dependent upon the number of neighbors (nn) included in each local estimate. Therefore, for each data set, L_{ave} was calculated for nn ranging from 4 to the total number of points in the data set. Then the relationship between L_{ave} and number of neighbors was examined. Small values of nn were insufficient for determining the local expansion rates λ_i. For a stochastic system, L_{ave} should decline to zero as nn increased to the total number of points in the data set, since the neighborhood would have less and less room to expand. For a deterministic system, however, there should be some region where L_{ave} was relatively constant, which would imply a constant expansion rate (Lyapunov exponent) was present. There is usually some noise present in most experimental systems, so in practice there will be three ranges of behavior: for very small nn, the noise is greater than the neighborhood size, and L_{ave} decreases logarithmically; for large nn, there is no room left to expand so L_{ave} again decreases logarithmically; and there should be some intermediate region where L_{ave} is constant. This technique provides a way of gauging the relative proportions of noise and determinism in the system's global behavior.

Unstable Periodic Orbits. UPOs were detected with a transform technique that concentrated the data around UPOs.[28] For period-1 orbits, the transformation was defined as

$$\hat{\mathbf{x}} \equiv [\mathbf{I} - \mathbf{S}(\mathbf{x},\mathbf{R})]^{-1} \cdot [\mathbf{F}(\mathbf{x}) - \mathbf{S}(\mathbf{x},\mathbf{R}) \cdot \mathbf{x}], \qquad (2)$$

where $\mathbf{x}$ was the d-dimensional time-delay vector of IBIs, $\mathbf{I}$ was the identity matrix, $\mathbf{F}(\mathbf{x})$ was a vector of the next iterate of $\mathbf{x}$, and $\mathbf{S}(\mathbf{x},\mathbf{R})$ was a $d \times d$ matrix function of $\mathbf{x}$ and a $d \times d \times d$ random tensor $\mathbf{R}$ given by

$$\mathbf{S}(\mathbf{x},\mathbf{R}) = \nabla \mathbf{F}(\mathbf{x}) + \mathbf{R} \cdot [\mathbf{F}(\mathbf{x}) - \mathbf{x}]. \qquad (3)$$

Here $\nabla \mathbf{F}(\mathbf{x})$ was the $d \times d$ Jacobian matrix of $\mathbf{F}(\mathbf{x})$, which was calculated using a least-squares fit of three spatial nearest neighbors (i.e., the nearest three points in state space). This transform was applied to every point $\mathbf{x}$ in the set and summarized in a one-dimensional (two-dimensional for higher-period orbits) spatial distribution function of the experimental data approximated by a histogram with a bin size of 0.02 s. The transformation shifted all points in the linear region of a fixed point $\mathbf{x}^*$ even closer to $\mathbf{x}^*$, thus creating a peak in the distribution function $\hat{\rho}(\hat{x})$. At any one value of $\mathbf{R}$, the transformation produced spurious peaks; these were filtered out by averaging $\hat{\rho}(\hat{x})$ over several (300) different values of $\mathbf{R}$. The higher the magnitude of $\mathbf{R}$, the more the peaks were smoothed out and the lower their amplitude.

For this analysis, amplitude-adjusted Fourier transform (AAFT) surrogates were used.[32] Fifty surrogate data sets were generated and transformed, and their corresponding probability distributions were calculated and averaged together. A cumulative histogram of the maximum deviation of each surrogate from the surrogate mean at each point was used to estimate the probability

that a peak in the transformed data was due to the presence of a true UPO at that point. To account for nonstationarity of the data (i.e., drifting of the mean IBI length) due to factors such as fatigue of the neurons, network plasticity, or fluctuations in temperature and pressure, each set of data was divided into windows of 256 IBIs and then analyzed. The selection of window size was based on optimizing the probability of finding a UPO (more points) while minimizing the amount of nonstationarity (fewer points).

It has been suggested that this detection algorithm might produce spurious UPO detections where there are actually none (T. Schreiber). To further ensure that the UPOs detected were truly significant, another surrogate test was devised. Data surrogates were produced and then analyzed as if they were experimental data, i.e., the UPO transform was applied to the surrogate and 50 surrogates of that surrogate and the significance of peaks in the histograms was calculated. This was done for five surrogates (both SS and AAFT) of each data set on 14 of 29 experiments. An estimate of the probability of finding a significant (i.e., $p < 0.05$) peak in each window was calculated for the data and the surrogates by dividing the number of windows with significant peaks by the total number of windows in each set. Then these probabilities were compared (data versus average of surrogates for that data set) using a paired t test to determine whether there was a significantly higher probability of finding a UPO in the data than in the surrogates. Naturally, 5% of surrogate windows were expected to have significant peaks in them since we used $p < 0.05$ as our significance criterion. Therefore, an experiment was considered significant if more than 5% of its windows contained a significant peak.

The selection of certain parameters such as embedding dimension (2) and number of nearest neighbors used for calculating the Jacobian (5) was not optimized, but corresponded to the conventional values used.[27] It is possible that the dynamics of the system are actually higher dimensional, and that UPO detection statistics might improve if a higher embedding dimension were used. However, there was a practical limit (due to finite data length, nonstationarity, and computation time) on how many dimensions one could use. The number of nearest neighbors used could ideally also be optimized: the use of too few or too many may cause the fit to be poor.

RESULTS

Generation of Spontaneous Bursting

An example of a typical spontaneous burst recorded extracellularly in the CA3 *stratum pyramidale* of a transverse hippocampal slice bathed in high-$[K^+]_o$ is shown in Fig. 1(A). Burst duration was typically between 30 and 60 ms. Once initiated, spontaneous bursting usually continued for at least 1 h. Typical burst trains for each of the three experimental techniques are shown in Figs. 1(B)–1(D). Both morphology and burst duration were consistent for all three induction protocols. The system state information was encoded as interburst intervals (IBIs) as seen in Fig. 1(B). The IBIs for the three bursting protocols had means and standard errors of 3.59 ± 0.54 s ($n = 16\,742$), 6.30 ± 0.44 s ($n = 3566$), and 6.37 ± 1.00 s ($n = 5741$) for experiments using high-$[K^+]_o$, zero-$[Mg^{2+}]_o$, and GABA$_A$ blockade, respectively.

Expansion Rate Analysis: No Evidence of Determinism

The issue of whether the spontaneous bursting was chaotic was first examined by calculating Lyapunov exponents for experiments using all three epilepsy models. The initial method used[12] evaluated the relationship between S (the average distance that two neighboring points will diverge after time τ) and τ for each experiment. The Lyapunov exponent (λ) was obtained by determining the slope of the least-squares fit line. However, upon closer inspection, it was noted that in all experiments, the neighborhoods expanded to well over half the size of the attractor within $\tau = 2$ time steps. An example of this rapid expansion is shown in Fig. 2. The least-squares fit could only include three points, making this method unreliable and necessitating the development of the short-time expansion technique. The presence of determinism was assessed by searching for plateaus in the curves of L_{ave} vs nn. These flat regions would indicate some measure of invariance in the expansion rate, which is expected for a chaotic system.

The short-time expansion technique was first tested on 1000 iterates of the Hénon map (delay embedded in two dimensions) with and without added noise and on five SS surrogates of these data. As seen in Fig. 3(A), L_{ave} for the curve of the average of the surrogates decreases uniformly to zero (open circle), while the curve of the Hénon map without noise (dark circle) is roughly horizontal. The Hénon map with noise (dark square) $\sigma = 0.02$ has a large plateau area in the range nn$= 3\% - 10\%$ (of the points in the attractor), and the curve for $\sigma = 0.2$ (dark triangle) has a smaller "shoulder" in the range nn$= 10\% - 20\%$. L_{ave} is reasonably close (0.50) to the accepted value of the maximal Lyapunov exponent for the Hénon map (0.41, dashed line). Note that as the noise amplitude increases, the curve becomes more and more like the curve of the surrogates (open circle) and (open triangle).

This method was then used to analyze 12 sets of IBI data from high-$[K^+]_o$ and zero-$[Mg^{2+}]_o$ experiments and 5 SS surrogates of each data set. No plateau region was observed in any of the bursting data sets tested. The curve in Fig. 3(B) shows the experiment with the biggest
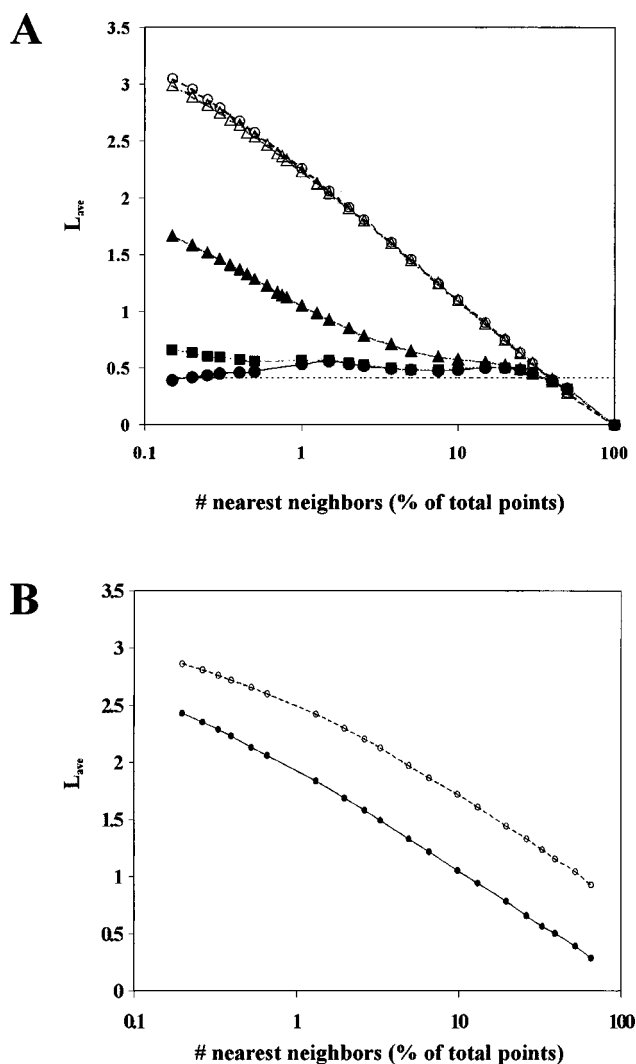
FIGURE 3. Dependence of L_{ave} on the number of nearest neighbors used (nn) for the Hénon map and data from a high-$[K^+]_o$ experiment. (A) Curves of L_{ave} for the 2000-point Hénon map (●), the Hénon map with added Gaussian noise [(■), $\sigma=0.02$; (▲), $\sigma=0.2$], and Gaussian-shuffled (SS) surrogates for noiseless (○) and noisy (△), $\sigma=0.2$ Hénon map. L_{ave} for the surrogates decreases logarithmically with nn, but the noiseless and low-noise Hénon data curves are almost flat, and are close to the accepted largest Lyapunov exponent (0.415, dotted line). This shows an invariant expansion rate. With larger amounts of noise ($\sigma=0.2$), the curve mirrors the surrogates at small and large nn, but has a plateau in the nn=5%−20% range. (Number of nearest neighbors are shown as a percentage of the total points in the whole attractor.) (B) Curves of L_{ave} for one set (points) of high-$[K^+]_o$ experimental data and corresponding SS surrogates. Curves for both data (●) and surrogates (○) decline logarithmically to zero with increasing nn. Also, the slopes of the two curves are almost identical, with no plateaus evident. This indicates that the data are stochastic, although perhaps slightly less random than the surrogates. This experiment had the largest difference between data and surrogate L_{ave} curves; the rest had less distance between the curves.

difference between data and corresponding surrogate average. Even in this case, there is no noticeable flattening of the data curve; it is almost parallel with the surrogate mean curve. Other data curves displayed even greater similarity to their surrogates' curves. However, the curve in this case is displaced from the surrogates, which suggests that perhaps it is not quite as disordered as the surrogates. Thus, the results of this analysis suggest that globally the bursting data contain a great deal of noise with no determinism detectable by our measure of the global expansion rate.

Evidence of Unstable Periodic Orbits

To search for determinism on a local scale, the presence of unstable periodic orbits in the interburst interval data was assessed. Data from the same experiments employed in the Lyapunov exponent analysis were used. Additional data sets that were deemed too short to be used in the Lyapunov analysis (i.e., less than 900 IBIs) were also included. Data from each experiment were divided into windows of 256 consecutive IBIs (with a 128 IBI overlap between windows) to minimize any effects of nonstationarity on the analysis. The transform was performed on the data and 50 AAFT surrogates for each window. To reduce any possible bias related to surrogate choice, the same analysis was also performed using SS surrogates on several experiments.

Period-1 Orbits. A histogram of one window of the original (untransformed) IBIs from a high-$[K^+]_o$ experiment is shown in Fig. 4(A). Note that no discernible peak is shown at the location of the period-1 orbit. After the transform is performed on the data [Fig. 4(B)], a sharp peak in the data (solid line) is seen at the corresponding location of the period-1 orbit (1.98 s). The dashed line shows the histogram of the mean of the transformed surrogates. Note that the peak for the surrogates is much lower than that for the transformed IBI data. A UPO was declared statistically significant if the peak in the distribution function of the data (minus the surrogate mean) was greater than 95% of the maximal peaks of the transformed surrogates (minus the surrogate mean). Since the peak in Fig. 4(C) is above the 95% significance line, it marks the location of a true period-1 orbit at 1.98 s.

The results of period-1 orbit detection for all experiments are summarized in the first three rows of Table 1. The first and second columns show the total number of experiments and percentage of significant experiments, respectively, for each preparation. A window containing a significant peak was considered a significant window. Period-1 orbits were found in 71% of the 17 high-$[K^+]_o$ experiments, 25% of the eight zero-$[Mg^{2+}]_o$ prepara-
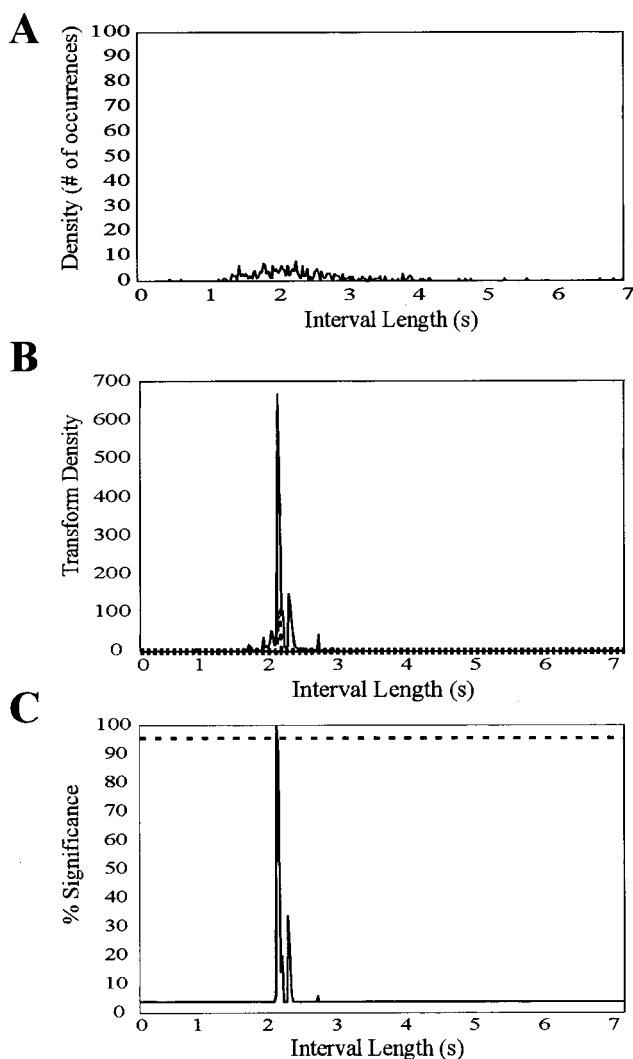
FIGURE 4. Detection of a period-1 orbit using the unstable periodic orbit (UPO) transform. (A) Histogram of the raw IBI data (from a high-$[K^+]_o$ experiment). Note that no large peaks are present. (B) Histogram of transformed data (solid) and mean of transformed surrogates (dotted). The peak in the data denotes possible fixed point. (C) Significance plot of the data seen in B with the surrogate mean subtracted. The 95% significance line is shown (dashed). The significance of the data at each IBI length is calculated by comparing the transformed data (minus the surrogate mean) to the cumulative histogram of the maximum peaks of the 50 transformed surrogates (minus the surrogate mean). If the peak in the data at any one point is greater than that of 48 surrogates at that point, then it is said to be more than 95% significant. Thus this figure shows a fixed point at the location of that peak (1.98 s) with $p < 0.05$.

tions, and 75% of the eight GABA$_A$ blockade experiments. Due to nonstationarity, period-1 orbits emerged, drifted, and disappeared over the course of an experiment. Analysis using SS surrogates produced similar results (not shown). Further analysis using phase-randomized surrogates[32] produced results with even

higher percentages of significant experiments and windows (not shown).

To further ensure that the detected UPOs were not spurious, the transform technique then was applied to five surrogates (both SS and AAFT) of each data set on 14 of 29 experiments from all three preparations. The probability of finding a significant (i.e., $p < 0.05$) peak in each overlapping window for the data and the mean of five surrogates was calculated and compared using a paired t test. The probability was significantly higher in the actual data than in surrogates both for SS surrogates (mean data probability 0.28, mean surrogate probability 0.06, $p < 0.004$) and for AAFT surrogates (mean data probability 0.22, mean surrogate probability 0.07, $p < 0.004$). As expected, the probability of finding a significant peak in a surrogate was approximately 0.05. This implies that the UPOs detected in the data were true UPOs, not "false positives."

Higher-Period Orbits. The case for chaos is made even stronger when orbits of higher periods are considered. Therefore, the same sets of experimental data were analyzed for period-2 orbits. A typical period-2 orbit is revealed in Fig. 5(A) by peaks at the two points of the orbit, both of which are higher than the 95% significance line. The results for period-2 detection are summarized in the last three rows of Table 1. Period-2 orbits were found in 35% of the high-$[K^+]_o$ experiments, 50% of the zero-$[Mg^{2+}]_o$ experiments, and 50% of the GABA$_A$ antagonist experiments. Overall, 73% of all experiments contained at least one period-1 or period-2 orbit. Significant period-3 orbits were also found in these experiments. Period-3 orbits [Fig. 5(B)] were found in data from all three epilepsy models. The location of the points along a higher-period orbit can be depicted using a return map (Fig. 6), which plots the current IBI vs the previous IBI. The significance in this three-dimensional representation of a two-dimensional histogram is coded by color and height. The deep red peaks indicate points with transform densities of greater than 95% significance. Note the symmetry of the period-2 points about the identity line [white, Fig. 6(A)]. Figure 6(B) shows a window of data containing two period-3 orbits (each circled and connected in blue and green) as well as a period-1 orbit (circled in orange and lying on the diagonal).

DISCUSSION

Our results provide evidence of both determinism and randomness in epileptiform bursting using two different measures of nonlinear behavior to analyze three different epilepsy models. Unstable periodic orbits of periods one, two, and three were found to be highly prevalent in all three models. However, Lyapunov estimation did not show large differences between data and surrogates.

TABLE 1. Summary of UPO detection results for period-1 and period-2 orbits in experiments using the high-$[K^+]_o$, zero-$[Mg^{2+}]_o$, and GABA$_A$, antagonist models. Because data for UPO transforms were divided into windows of 256 IBIs, the percentage of these windows containing significant UPOs is also included.

	UPO period	Total No. of experiments	% significant experiments	Total No. of windows	% significant windows
High-$[K^+]$	1	17	70.6	62	29.0
Low-$[Mg^{2+}]$	1	8	25.0	16	12.5
Bicuculline + Picrotoxin	1	8	75.0	19	42.1
High-$[K^+]$	2	17	35.3	62	11.3
Low-$[Mg^{2+}]$	2	8	50.0	16	31.3
Bicuculline + Picrotoxin	2	8	50.0	19	20.1

Thus, the global averages do not offer evidence of determinism, but the local measure (UPO analysis) does offer evidence of determinism. While these results seem to present conflicting evidence, they might suggest that *in vitro* epileptiform bursting may contain local islands of determinism (UPO detection) within a globally stochastic sea (Lyapunov analysis). It is possible that the noise level of the system was so high that it drowned out the determinism even using global averages. This was seen in the Hénon system as well: when very high noise levels were added, Lyapunov estimation could not distinguish the determinism in the system (data not shown). It is conceivable that when the expansion rates are averaged over many neighborhoods, the effects of noise predominate over chaos and some structure on a local scale

may be lost. It might be interesting to examine what a distribution of the local expansion rates might look like in a data set and in surrogates.

Previously published studies have searched for evidence of chaos and determinism in epilepsy, as discussed in the introduction. The results presented here are the first to demonstrate the prevalence of higher-period UPOs in three different *in vitro* epilepsy models. These models are thought to correspond to three different possible pathophysiologies of epilepsy. High-$[K^+]_o$ raises the neuronal resting potential closer to threshold and has been measured in conjunction with seizures *in vivo*. Zero-$[Mg^{2+}]_o$ unblocks NMDA-receptor channels, thus modeling increased excitatory activity that is also believed to contribute to some forms of seizure activity.[33]
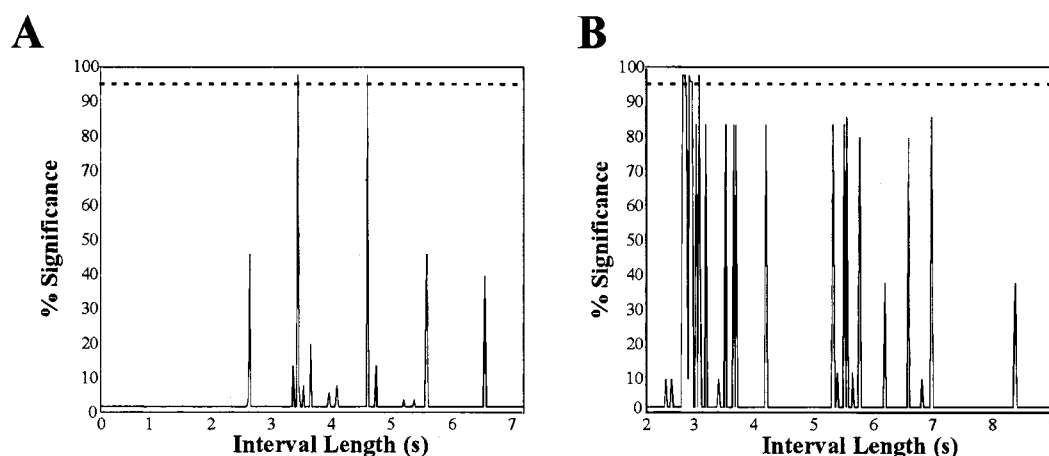
FIGURE 5. Detection of period-2 and period-3 orbits using the UPO transform. (A) One-dimensional significance plot of the period-2 transformed data from one window (256 consecutive IBIs) of a high-$[K^+]_o$ experiment. The two peaks rising above the 95% line denote the locations of the two points in a period-2 orbit. (B) One-dimensional significance plot of the period-3 transformed data from one window of a zero-$[Mg^{2+}]_o$ experiment. The three peaks rising above the 95% line denote the locations of the three points in a period-3 UPO. Note the existence of numerous secondary peaks below the 95% significance line, reflecting the greater difficulty of detecting UPOs as the period number increases.
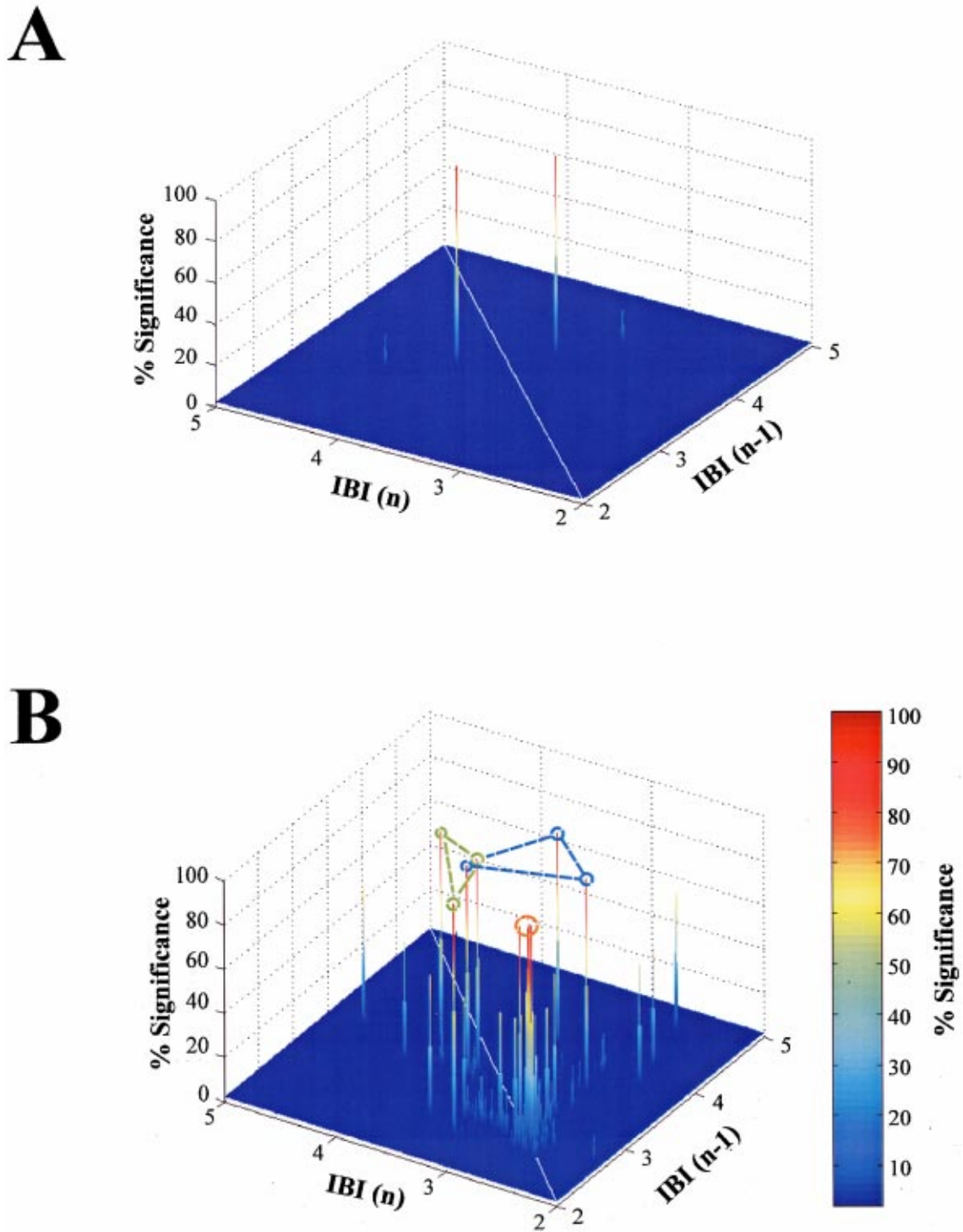
FIGURE 6. Period-2 and period-3 orbits in three-dimensional representations of two-dimensional state space. (A) Three-dimensional significance plot of a period-2 orbit from one window (256 consecutive IBIs) recorded during a high-$[K^+]_o$ experiment. The probability of the transformed data being outside the distribution of maximum peaks of 50 transformed surrogates is indicated by the color, as shown by the color bar on the right, and by the height, according to the scale on the z axis. The red peaks denote a period-2 orbit of greater than 95% significance. Note the symmetry across the identity line (in white). (B) Three-dimensional significance plot of two period-3 orbits from one window of a zero-$[Mg^{2+}]_o$ model. The two sets of three red peaks (circled in green and blue) manifest the three points along two period-3 orbits. The set of peaks circled in orange is a period-1 orbit.

Picrotoxin and bicuculline block GABA$_A$-mediated inhibition, yet another hypothesized cause of epileptic seizures.[5] Furthermore, this is the first calculation of global Lyapunov exponents for *in vitro* epileptiform bursting using surrogate data controls. The problem of inaccurate and false positive exponents when using older methods[21,34] was noted as a possible shortcoming of previous studies.[31] Those methods do not yield reliable estimates in short and noisy data sets. The algorithm developed by Kantz[12] is robust to a small amount of noise, but is not useful in the case of extremely rapid expansion or smaller data sets (as in the present study). The expansion technique used in this study was designed to counteract the effect of noise by averaging over all the points in each data set. It also compensates for the problem of nonstationarity by examining L_{ave} for multiple values of the number of nearest neighbors. Because it measures the expansion rate after only one iteration, the result is not, strictly speaking, the largest Lyapunov exponent. However, with such rapid expansion this method was the only way to assess whether the system was expanding deterministically or stochastically. The fact that the curves for the data were almost identical to those of the surrogate means suggests that the bursting contains a large stochastic component, though effects of higher-dimensional chaos or nonstationarity cannot be excluded. This is not surprising, since most biological systems have some amount of noise in them. The hippocampal slice preparation itself may have introduced a great deal of noise into the system. It is possible that in an intact brain, the many external inputs into the hippocampus may act to reduce the stochastic component, thus making the determinism easier to detect.

The most common form of epileptic seizures, complex partial seizures, are also the most likely to be refractory to medical treatment. Complex partial seizures often originate in the hippocampus, and hence the hippocampus is the region of the brain most often used to study epilepsy *in vitro*. The fact that deterministic behavior was found in three different *in vitro* epilepsy models in this region of the brain suggests that this behavior is intrinsic to interictal bursting. There exists some evidence based on UPO analysis[13,27] that interictal spikes generated in humans behave deterministically as well. If this is indeed true, then it might eventually be possible to apply chaos control to manipulate interictal spikes *in vivo*. Furthermore, two recent studies have demonstrated the ability to predict seizure activity several minutes before they occur.[14,15] While the precise role of interictal spikes in epileptogenesis is not yet certain,[4] it is plausible that developing a method to control them could provide a way to revert or perhaps prevent seizure activity as well.

The presence of unstable periodic orbits strengthens the rationale for using chaos control techniques to manipulate bursting, since UPOs are the points around which control can be applied.[24] However, the relatively large component of randomness detected suggests that chaos control may be difficult to achieve in practice. While chaos control techniques have been shown to have some success in controlling stochastic systems,[7] they would likely have trouble if the amplitude of the noise is larger than the region of state space to which control is desired. The presence of periodic orbits in a system indicates that the system contains determinism. When these periodic orbits are unstable, this provides necessary (though not sufficient) evidence of chaos as well. Thus, while we did not *irrefutably* detect chaos in these epilepsy models, we did find evidence *suggestive* of chaotic behavior.

NOMENCLATURE

AAFT: amplitude-adjusted Fourier transform
ACSF: artificial cerebrospinal fluid
CA: cornu ammonis
GABA: γ-amino-butyric acid
IBI: interburst interval
NMDA: *N*-methyl-*D*-aspartate
UPO: unstable periodic orbit
IPSP: inhibitory postsynaptic potential

REFERENCES

[1] Abarbanel, H. D. I., R. Brown, J. J. Sidorowich, and L. S. Tsimring. The analysis of observed chaotic data in physical systems. *Rev. Mod. Phys.* 65:1331–1392, 1993.

[2] Aitken, P. G., T. Sauer, and S. J. Schiff. Looking for chaos in brain slices. *J. Neurosci. Methods* 59:41–48, 1995.

[3] Auerbach, D., P. Cvitanovic, J.-P. Eckmann, G. Gunaratne, and I. Procaccia. Exploring chaotic motion through periodic orbits. *Phys. Rev. Lett.* 58:2387–2389, 1987.

[4] Barbarosie, M. and M. Avoli. CA3-Driven hippocampal-entorhinal loop controls rather than sustains *in vitro* limbic seizures. *J. Neurosci.* 17:9308–9314, 1997.

[5] Bradford, H. F. Glutamate, GABA, and epilepsy. *Prog. Neurobiol. (Oxford)* 47:477–511, 1995.

[6] Casdagli, M. C., L. D. Iasemidis, J. C. Sackellares, S. N. Roper, R. L. Gilmore, and R. S. Savit. Characterizing nonlinearity in invasive EEG recordings from temporal lobe epilepsy. *Physica D* 99:381–399, 1996.

[7] Christini, D. J., and J. J. Collins. Controlling nonchaotic neuronal noise using chaos control techniques. *Phys. Rev. Lett.* 75:2782–2785, 1995.

[8] Cvitanovic, P. Invariant measurement of strange sets in terms of cycles. *Phys. Rev. Lett.* 61:2729–2723, 1988.

[9] Ding, M. Z., and W. M. Yang. Deterministic point processes generated by threshold crossings: Dynamics reconstruction and chaos control. *Phys. Rev. E* 55:2397–2402, 1997.

[10] Dolan, K., A. Witt, M. L. Spano, A. Neiman, and F. Moss. Surrogates for finding unstable periodic, orbits in noisy data sets. *Phys. Rev. E* 59:5235–5241, 1999.

[11] Jerger, K., and S. J. Schiff. Periodic pacing an *in vitro* epileptic focus. *J. Neurophysiol.* 73:876–879, 1995.

[12] Kantz, H. A robust method to estimate the maximal Lyapunov exponent. *Phys. Lett. A* 185:77–87, 1994.

[13] Le Van Quyen, M., J. Martinerie, C. Adam, and F. J. Varela. Unstable periodic orbits in human epileptic activity. *Phys. Rev. E* 56:3401–3411, 1997.

[14] Lehnertz, K., and C. E. Elger. Can epileptic seizures be predicted? Evidence from nonlinear time series analysis of brain electrical activity. *Phys. Rev. Lett.* 80:5019–5022, 1998.

[15] Martinerie, J., C. Adam, M. Le Van Quyen, M. Baulac, S. Clemenceau, B. Renault, and F. J. Varela. Epileptic seizures can be anticipated by nonlinear analysis. *Nature Med.* 4:1173–1176, 1998.

[16] Pedley, T. A., and R. D. Traub. Physiological basis of the EEG. In: Current Practice of Clinical Electroencephalography, edited by D. D. Daly and T. A. Pedley. New York: Raven, 1990, pp. 107–137.

[17] Pei, X., and F. Moss. Characterization of low-dimensional dynamics in the crayfish caudal photoreceptor. *Nature (London)* 379:618–621, 1996.

[18] Pijn, J. P., J. Van Neerven, A. Noest, and F. H. Lopes da Silva. Chaos or noise in EEG signals; dependence on state and brain site. *Electroencephalogr. Clin. Neurophysiol.* 79:371–381, 1991.

[19] Rapp, P. E. Chaos in the neurosciences: Cautionary tales from the frontier. *The Biologist* 40:89–94, 1993.

[20] Rutecki, P. A., F. J. Lebeda, and D. Johnston. Epileptiform activity induced by changes in extracellular potassium in hippocampus. *J. Neurophysiol.* 54:1363–1374, 1985.

[21] Sarnthein, J., H. D. I. Abarbanel, and H. Pockberger. Nonlinear analysis of epileptic activity in rabbit neocortex. *Biol. Cybern.* 78:37–44, 1998.

[22] Sauer, T. Interspike interval embedding of chaotic signals. *Chaos* 5:127–132, 1995.

[23] Schiff, S. J., K. Jerger, T. Chang, T. Sauer, and P. G. Aitken. Stochastic versus deterministic variability in simple neuronal circuits. II. Hippocampal slice. *Biophys. J.* 67:684–691, 1994.

[24] Schiff, S. J., K. Jerger, D. H. Duong, T. Chang, M. L. Spano, and W. L. Ditto. Controlling chaos in the brain. *Nature (London)* 370:615–620, 1994.

[25] Schreiber, T., and A. Schmitz. Surrogate time series. *Physica D* 142:346–382, 2000.

[26] Shinbrot, T. Progress in the control of chaos. *Adv. Phys.* 44:73–111, 1995.

[27] So, P., J. Francis, T. I. Netoff, B. Gluckman, and S. J. Schiff. Periodic orbits: A new language for neuronal dynamics. *Biophys. J.* 74:2776–2785, 1998.

[28] So, P., E. Ott, T. Sauer, B. J. Gluckman, C. Grebogi, and S. J. Schiff. Extracting unstable periodic orbits from chaotic time series data. *Phys. Rev. E* 55:5398–5417, 1997.

[29] Strogatz, S. H. Nonlinear Dynamics and Chaos: With Applications to Physics, Biology, Chemistry, and Engineering. Reading, MA: Addison-Wesley Publishing, 1994, pp. 1–498.

[30] Takens, F. Detecting strange attractors in turbulence. In: Lecture Notes in Mathematics. New York: Springer, 1981, p. 898.

[31] Theiler, J. On the evidence for low-dimensional chaos in an epileptic electroencephalogram. *Phys. Lett. A* 196:335–341, 1995.

[32] Theiler, J., S. Eubank, A. Longtin, B. Galdrikian, and J. D. Farmer. Testing for nonlinearity in time series: The method of surrogate data. *Physica D* 58:77–94, 1992.

[33] Traub, R. D., J. G. Jefferys, and M. A. Whittington. Enhanced NMDA conductance can account for epileptiform activity induced by low Mg_2^+ in the rat hippocampal slice. *J. Physiol. (London)* 478:379–393, 1994.

[34] Wolf, A., J. B. Swift, H. L. Swinney, and J. A. Vastano. Determining Lyapunov exponents from a time series. *Physica D* 16:285–317, 1985.

[35] Yaylali, I., H. Kocak, and P. Jayakar. Detection of seizures from small samples using nonlinear dynamic system theory. *IEEE Trans. Biomed. Eng.* 43:743–750, 1996.